INSTITUTE OF PHYSICS PUBLISHING JOURNAL OF PHYSICS: CONDENSED MATTER

J. Phys.: Condens. Matter **18** (2006) 10509–10520 doi:10.1088/0953-8984/18/46/016

Crystal structure and relaxor-type transition in $SrBi_2Ta_2O_9$ doped with praseodymium

J Mata[1], A Durán[1], E Martínez[1,2], R Escamilla[3], J Heiras[1] and J M Siqueiros[1]

[1] Centro de Ciencias de la Materia Condensada, Universidad Nacional Autónoma de México, Apartado Postal 2681, Ensenada, Baja California, 22800, Mexico
[2] Centro de Investigación en Materiales, DIP-CUCEI, Universidad de Guadalajara, Apartado Postal 2-638, CP. 44281, Guadalajara, Jalisco, Mexico
[3] Instituto de Investigaciones en Materiales, Universidad Nacional Autónoma de México, México, DF, 04510, Mexico

Received 29 June 2006, in final form 17 October 2006
Published 3 November 2006
Online at stacks.iop.org/JPhysCM/18/10509

Abstract

The effects of Pr substitution in the structure and ferroelectric response for the $Sr_{1-x}Pr_xBi_2Ta_2O_9$ (SBT-Pr) compound have been studied. Rietveld refinement of the x-ray diffraction patterns indicates that the Pr ion progressively replaces the Sr site in the $A2_1am$ space group structure. The solubility of Pr in solid solution is around 15%. The replacement induces a change in the crystal structure and, as a consequence, the dielectric properties are affected. The ferroelectric transition at $T_m \sim 558$ K is shifted to lower temperatures, $T_m \sim 413$ K for $x = 0.15$ composition. Apparently, the tilt angle (α) associated with the c-axis does not play an important role since it remains essentially constant. However, the rotation in the ab-plane (β) as well as the octahedral distortion observed are strongly related to the coupling between T_m and x. A relaxor-type transition is observed as Pr is increased, leading to polar microregions above the nominal ferroelectric transition. The local disorder induced by the Pr ion is confirmed by the continuous increase in the diffuseness coefficient according to Isupov's model. These facts hinder the displacement of the TaO_6 octahedra with respect to Bi_2O_2 along the polarization axis, decreasing the polarization values.

(Some figures in this article are in colour only in the electronic version)

1. Introduction

$SrBi_2Ta_2O_9$ (SBT) was discovered at the beginning of the 1960s [1, 2]. It is a ferroelectric material that has recently attracted much interest as an unleaded alternative for PZT in ferroelectric non-volatile memory devices (FeRAM). SBT presents very good fatigue endurance, lower switching voltages and small polarization values [3, 4]. The crystal structure of SBT can be described as a stacking of layers of Bi_2O_2 separated by a double layer of tilted

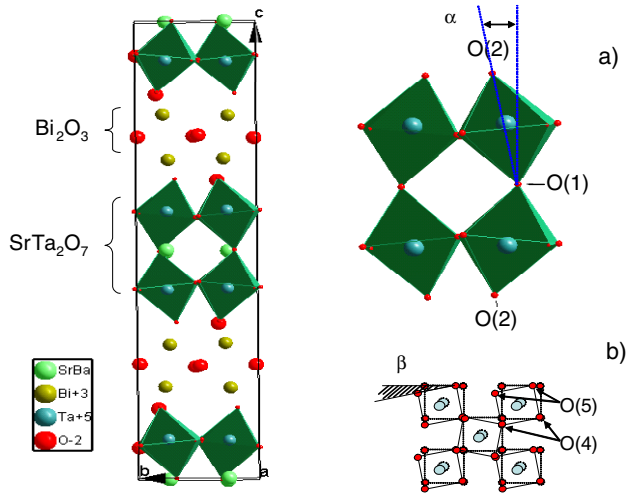

Figure 1. Crystal structure of distorted $SrBi_2Ta_2O_9$ showing (a) the tilting TaO_6 octahedra along the *c*-axis and (b) the rotation angle between adjacent octahedra in the *ab*-plane.

TaO_6 octahedra along the *c*-axis. The Bi_2O_2 layers are constituted by four different Bi–O(3) bond lengths while the TaO_6 octahedra by six different Ta–O bond lengths. These octahedra are corner-connected by the oxygen site O(1), and the tilt is clearly apparent from the O(2)–O(1)–O(2) bond angle of two adjacent octahedra as seen in figure 1(a). The Sr occupies the cavity between the octahedra [5, 6].

It was believed that the bismuth oxide layers were hard to modify, while the perovskite blocks were able to accommodate a large variety of cations. Recently, using techniques such as x-ray synchrotron radiation and a combination of standard x-ray and high resolution neutron powder diffraction data [7–9], it has been established that there is a significant degree of Sr^{2+}/Bi^{+3} cation disorder in the isostructural $ABi_2(Nb, Ta)_2O_9$ compounds and that this amount of disorder is essential for the stabilization of the Aurivillius structure. These results showed that the effective valence of the A site is, especially for Ba^{2+} and Sr^{2+}, noticeably greater than the nominal valence (2+), suggesting that the Sr site may accept, at least in part, higher valence (3+) cations while keeping the structure unchanged. Forbess *et al* [10] and Millan *et al* [11] studied the substitution of La^{3+} and Ca^{2+} for the Sr ion and the stereochemically active lone pair electrons such as Pb^{2+}, Sb^{3+} and Te^{4+} in the Bi_2O_2 layer of the $SrBi_2Nb_2O_9$ (SBN) compound. It was found that the SBN structure is preserved for such substitutions and that dielectric and spontaneous ferroelectric polarization vary notably with the substitution of alternative cations. On the other hand, Nogouchi *et al* [12–14] have demonstrated that higher valence cations like Bi and rare earths (such as La, Ce, Pr, Nd and Sm) at the A site with Sr vacancies modify substantially the SBT properties. It is found that the partial substitution of Sr by Bi ions increases the temperature at which the maximum of permittivity (T_m) occurs from 568 to 678 K, and improves the ferroelectric properties for the SBT compound. In contrast, the smaller ionic radii of rare earths give rise to a decrease of T_m and improve the spontaneous polarization. These studies have also shown that 20% of Pr ions and 50% of La ions with one-third of created vacancies in the solid solution lower T_m to 533 and 453 K, respectively. The delicate balance between vacancies and rare earth doping improves the polarization value in the SBT ceramic compound.

Although the SBT-Pr system has been investigated very recently, its systematic structural and dielectric response for low Pr content ($x < 0.2$) has still not been studied. This work deals with the study of the crystalline structure and the solubility limit for praseodymium in

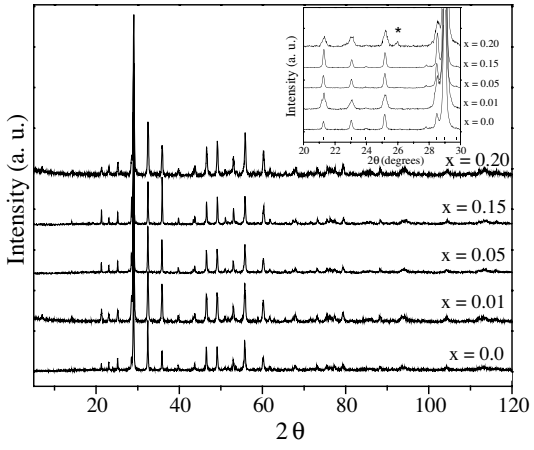

Figure 2. X-ray diffraction patterns for $Sr_{1-x}Pr_xBi_2Ta_2O_9$, $0 \leqslant x \leqslant 0.2$, powder samples at room temperature. The inset shows the region where a second phase is found (labelled *) for the $x = 0.2$ sample.

SBT samples prepared according to the formula $Sr_{1-x}Pr_xBi_2Ta_2O_9$ ($0 < x < 0.2$). Here the charge of the Pr ion was compensated assuming that partial substitution of a higher valence ion in the A site is necessary to stabilize the Aurivillius structure. The structural parameters are determined with good precision using Rietveld refinement analysis. Also, we analyse the nature of the phase transition through Isupov's model and a detailed study of the behaviour of the system as a function of composition is carried out for the first time.

2. Experimental details

Ceramic samples of $Sr_{1-x}Pr_xBi_2Ta_2O_9$ (SBT-Pr) with $x = 0$, 0.01, 0.05, 0.10, 0.15 and 0.20 were synthesized by solid-state reaction. Starting materials $SrCO_3$ (99.99%), Bi_2O_3 (99.99%), Ta_2O_5 (99.99%) and Pr_6O_{11} (99.9%) were mixed in stoichiometric proportions by ball milling. The resulting powders were calcined at 1173 K for 5 h, subsequently pressed into 1 cm diameter discs, placed in a crucible under a Bi_2O_3 controlled atmosphere and sealed with powdered alumina and finally sintered at 1523 K for 2 h. The measured density of the sintered samples was 95% of the theoretical density. Phase identification in the samples was carried out with a Siemens D5000 x-ray diffractometer using Cu Kα radiation and an Ni filter. Intensities were measured in steps of 0.02° for 14 s in the 2θ range of 5° to 120° at room temperature. The crystallographic phases were identified by comparison with the x-ray patterns of the JCPDS database. Crystallographic and structural parameters were refined by the Rietveld method using the QUANTO program [15] with multi-phase capability based on the $A2_1am$ orthorhombic symmetry.

Silver electrodes were placed on the discs of the polished ceramic samples. Capacitance measurements were carried out from room temperature up to 823 K in the frequency range of 10 kHz–1 MHz using an LCR bridge (HP-4284A) working at ten different frequencies. The hysteresis loop measurements were performed using an RT66A ferroelectric tester by Radiant Technologies Inc. at room temperature.

3. Results

3.1. Structural analysis

The XRD patterns in figure 2 show that the samples are single phase for $0 < x < 0.15$. A secondary phase appears only for $x = 0.20$. We also show, in the inset of figure 2, an

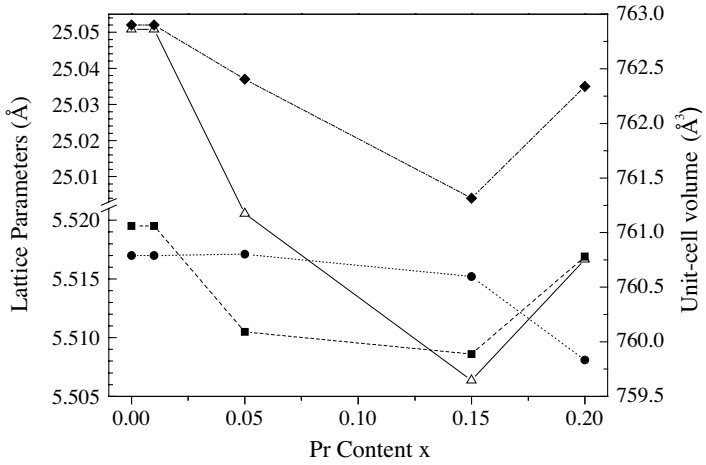

Figure 3. Crystal lattice parameters (a, b, c) and unit cell volume as functions of Pr-ion content (x) for $Sr_{1-x}Pr_xBi_2Ti_2O_9$.

amplification of the region where the $SrTa_2O_6$ (ICDD No 051-1683) compound, as second phase, was identified, indicating that the solubility limit is around 0.15 for Pr ions in solid solution. For lower Pr concentrations and taking into account the resolution limit of the Cu Kα conventional 2θ diffraction scan, the presence of fluorite or pyrochlore as second phases was discarded. As an example, a fitted pattern for the $x = 0.05$ sample was calculated. The obtained pattern assuming that the Pr ion is substituted in the Sr site, based on the $A2_1am$ orthorhombic symmetry, fitted well onto the experimental data. Detailed results of the structural refinement are listed in table 1. The first three rows show the trend of the lattice parameters at room temperature with the increase of Pr content. The occupancy (N) of the Sr/Pr ion was refined assuming that all sites were occupied ($N = 1$); the thermal parameter (B_{eq}) was fixed and, simultaneously, the occupancy and the B_{eq} were incorporated into the refining cycling. For $x = 0$, the lattice parameters are $a = 5.5195(3)$ Å, $b = 5.5170(4)$ Å and $c = 25.0520(2)$ Å, which are in good agreement with the reported data for SBT [16, 17]. It is observed that as x increases from 0 to 0.15 of Pr ion content the a, b and c lattice parameters decrease, and as a consequence of these changes the unit-cell volume also decreases, as can be clearly seen in figure 3. The orthorhombic distortion (b/a) increases from 0.9995 to 1.0012 in the range of $0 \leqslant x \leqslant 0.15$. The shrinkage of the unit cell may be explained in terms of the ionic radii of the Sr^{2+} (1.44 Å) and Pr^{3+}/Pr^{4+} ions (1.179 and 0.96 Å) [18]. Although the final refinement for further Pr content ($x = 0.20$) produced a relatively good fit to the data ($R_{wp} \sim 13.1\%$), the change of the tendency observed at $x = 0.15$ could be related to two facts: first, a second phase segregation in the sample, which also reveals the limit of Pr solubility in the structure; second, the presence of an intermediate phase of the SBT structure could be another factor to change the shrinkage tendency. It was demonstrated that a variant of the SBT compound was identified by high temperature powder neutron diffraction data showing an intermediate phase between ferroelectric ($A2_1am$) and paraelectric phases ($I4/mmm$) [19].

Recent x-ray photoelectron spectroscopy (XPS) [10] studies of SBT:Pr showed that the Pr ion is substituted at the Sr site as Pr^{3+}, unlike what happens in $Sr_{1-x}Pr_xTiO_3$ (STO:Pr), where mixed valence (Pr^{3+}/Pr^{4+}) is found [20]. In this context, an estimation of the valence of cations/anions present in the solid solution can be made for SBT-Pr by means of the Brown bond valence model [21, 22], which takes into consideration structural stress or covalence effects in

Table 1. Structural parameters obtained from Rietveld refinement for $Sr_{1-x}Pr_xBi_2Ta_2O_9$ for $0 \leqslant x \leqslant 0.20$ at 295 K. Numbers in parentheses indicate the standard deviation for the last significant digit. (Space group: $A21am$. Atomic positions: Bi, 8b (x, y, z); Sr, 4a $(0, y, 0)$; Ta, 8b (x, y, z); O(1), 4a $(x, y, 0)$; O(2), 8b (x, y, z); O(3), 8b (x, y, z); O(4), 8b (x, y, z); O(5), 8b (x, y, z).)

		$x = 0.0$	$x = 0.01$	$x = 0.05$	$x = 0.15$	$x = 0.2$
	a (Å)	5.5195(3)	5.5195(2)	5.5105(2)	5.5086(4)	5.5169(4)
	b (Å)	5.5170(4)	5.5170(3)	5.5171(3)	5.5152(2)	5.5081(3)
	c (Å)	25.052(2)	25.052(2)	25.037(3)	25.004(4)	25.035(4)
	b/a	0.9995	0.9995	1.0001	1.0012	0.9984
	V (Å^3)	762.86	762.90	760.41	759.64	760.75
Bi	x	0.4634(2)	0.4638(2)	0.4645(3)	0.4663(5)	0.4634(3)
	y	0.7764(1)	0.7763(1)	0.7759(2)	0.7750(2)	0.7764(3)
	z	0.1999(2)	0.1999(2)	0.1999(1)	0.200(1)	0.1999(2)
	B (Å^2)	1.13(3)	1.08(3)	0.91(4)	0.98(4)	1.02(4)
Sr/Pr	y	0.2567(3)	0.2566(4)	0.2561(2)	0.2550(2)	0.2567(2)
	B (Å^2)	0.7(1)	0.7(1)	0.19(1)	0.11(2)	0.13(1)
	N	0	0.007(2)	0.055(2)	0.12(1)	0.17(2)
Ta	x	0.5104(2)	0.5104(3)	0.5105(4)	0.5106(5)	0.5104(3)
	y	0.7480(2)	0.7480(2)	0.7480(3)	0.7479(3)	0.7480(3)
	z	0.4148(4)	0.4148(3)	0.4149(3)	0.4150(2)	0.4148(1)
	B (Å^2)	0.05(3)	0.11(3)	0.21(4)	0.20(4)	0.08(4)
O(1)	x	0.5248(2)	0.5247(2)	0.5243(1)	0.5234(2)	0.5248(2)
	y	0.2892(4)	0.2893(3)	0.2898(4)	0.2911(4)	0.2892(4)
	B (Å^2)	1.7(9)	2.4(9)	0.81(3)	1.2(7)	0.87(1)
O(2)	x	0.5219(4)	0.5219(4)	0.5217(4)	0.5212(4)	0.5219(3)
	y	0.6990(2)	0.6989(4)	0.6985(3)	0.6974(4)	0.6990(4)
	z	0.3418(3)	0.3418(3)	0.3418(2)	0.3418(3)	0.3419(5)
	B (Å^2)	0.6(5)	1.4(6)	2.9(7)	3.0(1)	0.63(3)
O(3)	x	0.7381(2)	0.7381(1)	0.7382(2)	0.7385(1)	0.7381(2)
	y	0.9923(2)	0.9923(2)	0.9923(4)	0.9924(4)	0.9923(4)
	z	0.2507(1)	0.2507(1)	0.2508(3)	0.2507(3)	0.2508(3)
	B (Å^2)	4.4(7)	3.1(7)	4.7(8)	4.0(2)	1.29(6)
O(4)	x	0.7554(3)	0.7553(3)	0.7549(2)	0.7538(3)	0.7554(3)
	y	0.9867(2)	0.9866(3)	0.9865(4)	0.98608(2)	0.9867(2)
	z	0.0696(2)	0.0696(2)	0.0696(2)	0.0695(1)	0.0696(2)
	B (Å^2)	0.7(4)	0.7(7)	0.6(2)	0.8(1)	0.78(2)
O(5)	x	0.7909(3)	0.7908(4)	0.7905(3)	0.7898(2)	0.7909(3)
	y	0.9807(2)	0.9806(2)	0.9804(2)	0.9799(2)	0.9807(1)
	z	0.5836(2)	0.5835(1)	0.5835(1)	0.5835(1)	0.5836(3)
	B (Å^2)	0.8(8)	0.7(7)	0.8(6)	1.1(7)	1.4(1)
	R_p (%)	9.8	9.9	6.4	7.7	10.2
	R_{wp} (%)	12.5	12.6	10.8	13.6	13.1
	R_{exp} (%)	7.0	7.1	3.8	3.9	8.6
	χ^2 (%)	1.7	1.8	2.8	3.4	1.5

the crystal by mean of a single parameter GII, the global instability index of the bond-valence model [21]. In this model (derived from Pauling's rules), an empirical correlation is used to determine the bond valence between two atoms i and j, s_{ij}, of a chemical bond from its length referred to as the *bond valence parameter*, R_{ij}:

$$s_{ij} = \exp((R_0 - R_{ij})/B) \tag{1}$$

where $B = 0.37$ and R_0 is the length of a bond of unit valence. The values of R_0 for most of the common bonds are tabulated in [18].

For most compounds it is found that the sum of the bond valences around any atom, i, is equal (or nearly equal) to its valence or oxidation state, V_i:

$$\Sigma s_{ij} = V_i. \tag{2}$$

In practice, equation (2) will rarely be exactly obeyed because of uncertainties in the measured bond length, but the difference between the bond-valence sum (BVS) and the atomic valence is usually small (<0.1 valence units (vu)) unless lattice effects cause excessive stretching or compression of the bonds. Where such lattice strains occur, as they do frequently in the perovskites, it is convenient to measure them in terms of the discrepancy, d_i:

$$d_i = V_i - \Sigma s_{ij}. \tag{3}$$

A measure of such lattice strains over the whole structure is the global instability index, GII, which is the root mean square average of the d_i-values:

$$\mathrm{GII} = \langle d_i^2 \rangle^{1/2}. \tag{4}$$

Larger values of d_i and GII are indicative of strained bonds, which can lead to instabilities in the crystal structure. For unstrained structures GII < 0.1 vu, but for compounds with lattice-induced strains GII can be as large as 0.2 vu. Crystal structures with GII > 0.3 vu are generally found to be either incorrect or refined in a space group with too high a symmetry [20]. This model gives a phenomenological relationship between the formal valence of a bond and the corresponding bond length.

Table 2 contains a selected list of bond lengths, octahedral distortion (Δ_{oct}) and angles of the TaO_6 octahedra and Bi_2O_3 layer for SBT-Pr. It is worth noting that, very likely, the position and the possible oxygen-atom displacement were not accurately determined from the standard x-ray data. However, the refined data obtained here coincided with those reported previously [7, 23]. Thus, the data reveal that the TaO_6 octahedron is not perfect and it is distorted as a consequence of four different Ta–O bond lengths. The bond length between Ta and apical O(1) linking both octahedra (see figure 1(a)) is longer than the Ta and apical O(2) in the $SrTa_2O_7$ perovskite unit. Also, it is observed that one of the Ta–O(4) and Ta–O(5) is shorter than the other one. The effect of the Pr doping on this set of Ta–O bond lengths can be better visualized through the octahedral distortion Δ_{oct}, which decreases from 2.26 to 2.08 Å as Pr ion concentration is increased in the range of $0 \leqslant x \leqslant 0.15$. This finding reveals a tendency to pseudo-tetragonal structure as Pr is being incorporated in the structure. On the other hand, three kinds of Bi–O(3) bond lengths are smaller than the Shannon [18] ionic radii sum, of 2.36 Å, and the other Bi–O(3) is larger than expected. As mentioned above, the data strongly suggest that above 15% of Pr ions the bond lengths as well as the lattice parameter changes could be indexed in another space group of pseudo-tetragonal structure.

Table 3 lists the calculated valence for Sr, Pr, Bi, Ta and O from the individual Sr/Pr–O, Bi–O and Ta–O bond lengths listed in table 2. According to the BVS, the Bi site, Ta site and Pr site are undervalenced and the Sr site is overvalenced. As the Pr content is increased, the BVSs of the Bi site and Pr site approach the nominal valence 3+ in agreement with that obtained in [10] by XPS in the Pr-SBT compound. The Ta in the TaO_6 octahedron is 5+ and the Sr site becomes slightly further overvalenced. This enhancement of the Sr valence can be associated with the excess Pr^{3+} in the Sr site, and the undervalence of Bi to the presence of oxygen vacancies and/or substitution of Sr^{2+} in the Bi site in the structure. This double substitution has been observed by Blake *et al* [7], Ismunandar and Kennedy [8] and Macquart *et al* [9], in the isomorphic compounds $ABi_2Nb_2O_9$ and $ABi_2Ta_2O_9$ with A = Ba, Sr or Ca.

Table 2. Bond lengths (Å) and bond angles (degrees) for TaO_6 octahedra as well as the evaluated tilting (α) from the c-axis and the rotation (β) angles in the ab-plane for $Sr_{1-x}Pr_xBi_2Ta_2O_9$ with $0 \leqslant x \leqslant 0.20$ at 295 K. (The octahedral distortion is defined as $\Delta_{oct} = 10 \times (\Sigma|(M\text{–}O_i) - \langle M\text{–}O\rangle_{average}|)/\langle M\text{–}O\rangle_{average}$.)

	x				
	0.0	0.01	0.05	0.15	0.2
Ta–O(1)	2.148(2)	2.148(2)	2.145(3)	2.140(2)	2.147(3)
Ta–O(2)	1.847(3)	1.850(2)	1.850(3)	1.851(3)	1.846(2)
Ta–O(4)	1.952(2)	1.952(3)	1.951(3)	1.953(3)	1.950(3)
Ta–O(4)	2.015(3)	2.015(1)	2.011(2)	2.008(3)	2.013(2)
Ta–O(5)	1.926(1)	1.927(2)	1.928(2)	1.932(2)	1.924(2)
Ta–O(5)	2.012(2)	2.011(3)	2.007(2)	2.001(3)	2.010(1)
$\langle Ta\text{–}O\rangle_{average}$	1.989	1.984	1.982	1.981	1.982
Octahedral distortion (Δ_{oct})	2.26	2.24	2.19	2.08	2.27
Bi–O(3)	2.189(2)	2.191(2)	2.194(2)	2.197(1)	2.189(1)
Bi–O(3)	2.296(3)	2.297(2)	2.295(2)	2.295(4)	2.293(2)
Bi–O(3)	2.310(3)	2.309(1)	2.307(4)	2.300(2)	2.309(3)
Bi–O(3)	2.507(4)	2.505(2)	2.499(3)	2.489(4)	2.503(4)
Main and tilting angles of the TaO_6 octahedra					
O(4)–Ta–O(4)	88.31(2)	88.31(3)	88.25(2)	88.27(2)	88.37(2)
O(5)–Ta–O(5)	89.30(2)	89.30(3)	89.23(2)	89.24(1)	89.36(3)
O(4)–Ta–O(5)	93.30(1)	93.27(2)	93.29(1)	93.06(2)	93.25(2)
O(4)–Ta–O(5)	86.33(2)	86.35(1)	86.54(2)	86.76(3)	86.28(1)
Ta–O(1)–Ta	167.13(2)	167.11(2)	167.00(3)	166.66(2)	167.14(3)
β	4.41	4.44	4.49	4.60	4.41
Tilting angle (α)	7.25	7.18	7.25	7.45	7.16

Table 3. Bond valence sum (BVS) determined for $Sr_{1-x}Pr_xBi_2Ta_2O_3$ ceramic compounds.

	x				
	0.0	0.01	0.05	0.15	0.2
BV − sum of Sr (vu)	2.27	2.27	2.28	2.30	2.28
BV − sum of Pr (vu)	—	2.58	2.60	2.61	2.60
BV − sum of Bi (vu)	2.78	2.78	2.79	2.80	2.80
BV − sum of Ta (vu)	4.95	4.94	4.96	4.97	4.97
BV − sum of O1 (vu)	1.91	1.91	1.92	1.95	1.94
BV − sum of O2 (vu)	1.69	1.69	1.69	1.69	1.70
BV − sum of O3 (vu)	2.10	2.10	2.10	2.11	2.11
BV − sum of O4 (vu)	2.10	2.10	2.12	2.13	2.13
BV − sum of O5 (vu)	2.02	2.02	2.03	2.03	2.04
GII (vu)	0.18	0.22	0.22	0.21	0.21

On the other hand, for off-stoichiometry and doped SBT, Shimikawa *et al* [23] and Nogouchi *et al* [12] have focused their attention on the tilting angle away from the c-axis as well as the rotation in the ab-plane performed by the TaO_6 octahedra, which in some way improve the ferroelectric properties. In this work, these angles are depicted in figures 1(a) and (b). Rietveld refinement analyses revealed the following facts: the tilt angle (α) from the c-axis

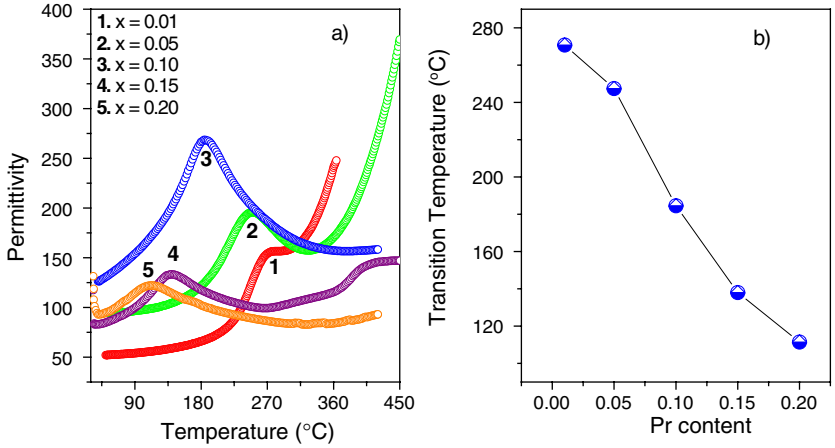

Figure 4. (a) Temperature dependence of $\varepsilon/\varepsilon_0$ at 1 kHz in $Sr_{1-x}Pr_xBi_2Ta_2O_9$ polycrystals. (b) Praseodymium content dependence of the transition temperature.

remains essentially constant with a value around 7.4° [O(2)–O(1)–O(2)] while the rotation of the TaO_6 octahedra (β) estimated from the angle formed by the [O(5)–O(5)–O(5)] in the *ab*-plane increases from 4.41° to 4.60° for $0.0 \leqslant x \leqslant 0.15$, which for $x = 0$ is consistent with an earlier report [12]. For higher Pr concentration, the rotation decreases to 4.41°, following the same tendency of the lattice parameter. Again, this result suggests a progressive introduction of the Pr ion into the solid solution with solubility limit around 15%; above this value, no more praseodymium is accepted in the system without departure from stoichiometry. All these parameters as well as the main angles are listed in table 2. This result is directly related to the preferential occupation of the smaller praseodymium ion at the Sr site responsible for the overall structure change. It is worthwhile to emphasize that this result is expected, because in this study 'defect engineering' is not performed from starting powders for stoichiometric compositions ($Sr_{1-x}Pr_{2/3x}Bi_2Ta_2O_9$). Thus, it is expected that the progressive introduction of Pr ion into the crystalline structure leads to notable changes in the dielectric and polarization properties, as is explained in the next part.

3.2. Dielectric behaviour

The temperature dependence of the dielectric constant for Pr-SBT samples at 1 kHz is shown in figure 4(a). The permittivity curves show a remarkable shift of the transition temperature (T_m) toward lower temperatures with increasing Pr content, from ∼553 to ∼393 K, with a roughly linear relation between T_m and x, as seen in figure 4(b). Such a shift is larger than that observed for the 20% Pr doped SBT ceramic sample studied in an earlier report [14]. In general, it is considered that the Sr vacancies play an important role regarding the magnitude of the permittivity at T_m and the coupling of T_m versus rare earth doping. Here, a strong coupling between T_m and Pr doping is observed; however, permittivity values around the ferroelectric transition are relatively low. Thus, we consider that the substitution for the smaller Pr ion is directly responsible for the coupling between T_m and x. These results allow us to conjecture that the introduction of Sr vacancies is the main cause for the increase in the magnitude of the permittivity around the ferroelectric–paraelectric transition as was observed in 20% Sm, 30% Nb and 50% La-modified SBT [12, 13]. Another remarkable characteristic is the broad phase transition indicative of a diffuse phase transition (DPT). As Pr enters at the Sr site a typical

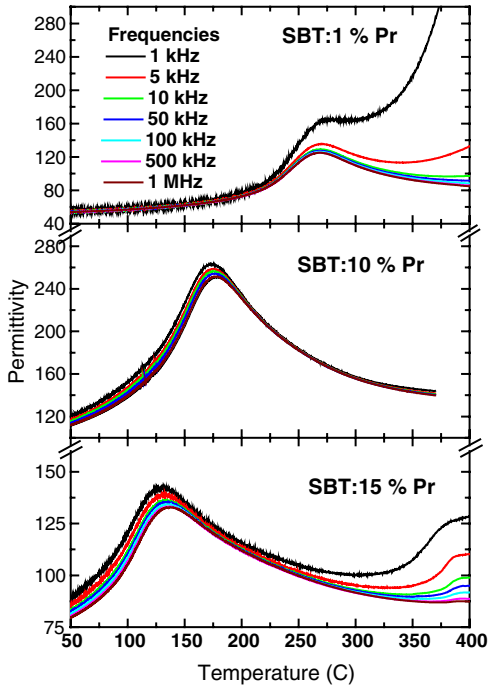

Figure 5. Permittivity versus temperature for 1, 10 and 15% of Pr doped in SBT at several frequencies.

relaxor behaviour is observed, as shown in figure 5. For 10% Pr in the solid solution, the magnitude of the dielectric constant decreases with increasing frequency and the maximum shifts toward higher temperature. This behaviour must be attributable to the existence of polar microregions above the nominal transition temperature, mainly as a consequence of a inhomogeneous distribution of the Pr ion at the Sr site, leading to local polarization fluctuations. Furthermore, we have measured the permittivity up to 1073 K in search of another possible polar signal at higher temperatures. The results showed a small hump at about 683 K for $x = 0.15$ and at 923 K for $x = 0.20$ samples. This signal could be due to the phase fluctuations of Bi deficient SBT growing as stacking faults in the layered structure sequence. The variability of the Pr, Sr/Bi site in the diluted limit could result in a variation of the SBT structure with respect to that of the stoichiometric SBT compound. This assumption is consistent with the fact that the $A2_1am$ is not an isotropic subgroup of the tetragonal $I4/mmm$, and several polar space groups such as $Fmmm$, $Amam$, $Aba2$ [6, 23, 24] could lead to the polar signal at higher temperature. Thus, for this latter composition we believe that a pseudo-tetragonal phase coexists with a negligible $SrTaO_6$ impurity as a second phase, leading to low dielectric values.

4. Discussion

4.1. Diffuse phase transition (DPT) in the $Sr_{1-x}Pr_xBi_2Ta_2O_9$ solid solution

A modified Curie–Weiss law [25] is often used to describe the diffuseness of the phase transition:

$$\frac{1}{\varepsilon} - \frac{1}{\varepsilon_{\max}} = \frac{(T - T_c)^\gamma}{2\delta^2 \varepsilon_{\max}} \tag{5}$$

where γ is assumed to be constant. The limiting values $\gamma = 1$ and 2 reduce the expression to the Curie–Weiss law valid for the case of a normal ferroelectric and to the quadratic dependence

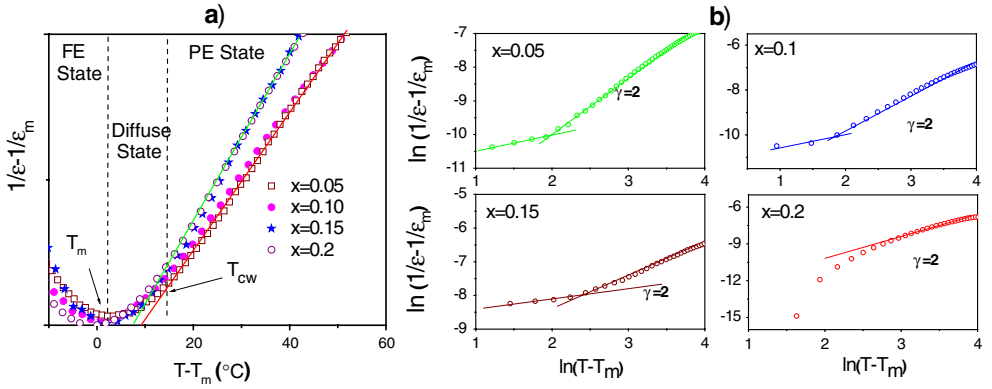

Figure 6. (a) The inverse dielectric constant $(1/\varepsilon - 1/\varepsilon_m)$ as a function of temperature at 1 kHz for $x = 0.05, 0.1, 0.15$ and 0.2 praseodymium content. The line represents the fit using the Curie–Weiss law. (b) $\ln(1/\varepsilon - 1/\varepsilon_m)$ as a function of $\ln(T - T_m)$ for SBT-Pr ceramics.

valid for an ideal diffusive ferroelectric, respectively. Figure 6(a) shows the inverse of the permittivity as a function of temperature at 1 kHz and the fits to the experimental data using the Curie–Weiss law ($\gamma = 1$). In these curves, three different regions may be distinguished: the ferroelectric state at temperatures below the temperature of maximum permittivity (T_m), the state where polar (micro/nano) clusters exist for temperatures between T_m and T_{cw} and the paraelectric state for temperatures above T_{cw}. The 'real' Curie temperature is obtained by the intersection of the linear extrapolation of the curve from the paraelectric state, where the Curie–Weiss law holds, with the temperature axis. T_m would then be the transition temperature of the material should it have a normal order transition instead of a phase transition with polar micro-/nanoclusters. In figure 6(b) $\ln(1/\varepsilon - 1/\varepsilon_m)$ versus $\ln(T - T_m)$ is plotted to show that the Curie–Weiss law does not hold and is not representative of the overall behaviour of the material. The regions where the Isupov law ($\gamma = 2$) is valid allow us to determine the disorder parameter (δ) using equation (5), plotting $(1/\varepsilon - 1/\varepsilon_m)$ against $(T - T_m)^2$ for all compositions (see figure 7(a)). The values for δ are reported in the same graph, where an increase in its value is observed with the increase in Pr content. This behaviour is explained by the higher disorder associated with the random location of the ions in the crystal sites when $Pr^{3+,4+}$ substitutes Sr^{2+}. The composition fluctuations will then be larger, originating a wider transition temperature distribution.

4.2. Ferroelectric properties

Figure 7 shows the polarization versus applied electric field at room temperature for the studied compositions. The spontaneous polarization for stoichiometric SBT is about 5.8 μC cm^{-2} [17, 26], in contrast to that observed in Sr-deficient and Bi-rich compounds such as $Sr_{0.8}Bi_{2.2}Ta_2O_9$, where the spontaneous polarization ($\sim$10, 18 μC cm^{-2}) is about twice as large as stoichiometric SBT. On the other hand, it is 70% higher than the value reported by Shimakawa *et al* [17]. Although the ferroelectric properties reported here are consistent with those of pure stoichiometric SBT, the progressive inclusion of praseodymium decreases the remanent polarization of SBT. Noguchi *et al* [14, 12], however, report higher values for 20% Pr-doped SBT. This is because Pr^{3+} occupies the Sr site plus 1/3A-site vacancies. This process enhances the stability of the ferroelectric phase and increases the polarization values. They have also observed an increase of the tilt angle of the TaO_6 octahedra along the c-axis ($\sim$7.9°),

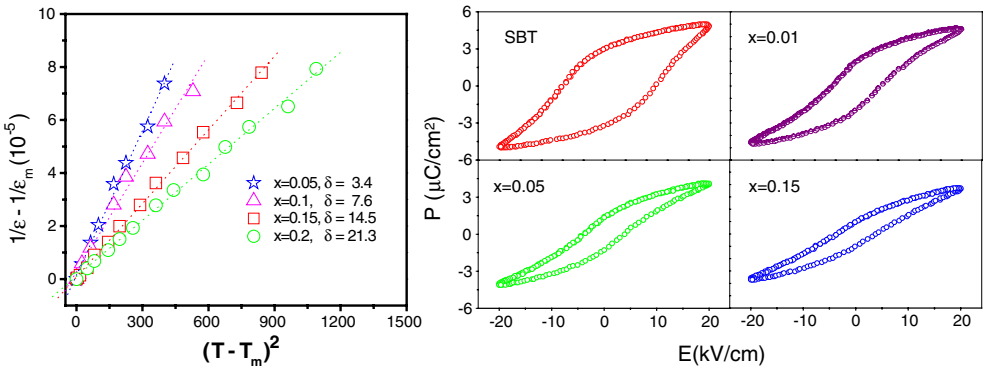

Figure 7. (a) $(1/\varepsilon - 1/\varepsilon_m)$ versus $(T - T_m)^2$ for all samples. In each case the diffusivity coefficient may be determined from the slope of the respective curve and equation (1). (b) Variations of the hysteresis loop with Pr content measured at 20 kV cm^{-1} for $x = 0.0$, 0.01, 0.05 and 0.15 praseodymium content.

enhancing the polarization values to about 18 μC cm^{-1}. Here, the substitution of Pr ions for divalent Sr ions slightly enhances the rotation of the TaO_6 octahedra around the c-axis without considerable changes in the tilting angle along the c-axis (∼7.4°), probably because the Pr ions increase the local covalence in the perovskite block since the average ⟨Ta–O⟩ bond length decreases from 1.989 to 1.981 Å as doping is increased from 0 to 15% of Pr ion. On the other hand, the octahedral distortion decreases as Pr concentration is increased in the solid solution. These facts suggest that the perovskite block tends to maintain the perovskite ideal form. However, a considerable shift of T_c towards lower temperatures is probably related to the rotation angle around the c-axis in the $(Sr_{1-x}Pr_x)$ SBT structure. At first sight, the introduction of vacancies is apparently an important condition for having higher polarization values due to a larger tilting angle distortion along the c-axis. Although in this work the vacancies within the crystalline structure are not considered, studies to optimize vacancy density for 0.15% Pr doping to obtain low transition temperatures and high polarization values are in progress.

5. Conclusions

We have synthesized $Sr_{1-x}Pr_xBi_2Ta_2O_9$ with $x = 0$, 0.01, 0.05, 0.15 and 0.20 samples and examined their crystal structure and ferroelectric properties. The modified SBT is single phase in the $0 \leqslant x \leqslant 0.15$ composition range. In contrast with the behaviour of Pr in the STO:Pr compound, in SBT:Pr, Pr acts as single valent with a 3+ valence. The contribution of the displacement between TaO_6 octahedra and Bi_2O_2 layers to the remnant polarization is about 30% lower than in the undoped SBT compound. The ε versus T curves show broad phase transitions typical of disordered systems, as is revealed through the analysis of the phase transition with Isupov's model. The 1% Pr sample was particularly interesting, presenting an almost symmetrical ε versus T curve around T_m, indicative of a low loss sample at high temperatures. The relative permittivity values at room temperature were around 50–100, which are reasonable values for standard capacitors. A considerable shift toward lower values of the transition temperature with Pr concentration is observed. An increase of the disorder is found with the increment of Pr content, reaffirming that its substitution enhances the structural disorder, increasing therefore the diffuse character of the transition, resulting in the loss of the long-range ferroelectric ordering. The hysteresis loop indicates that the substitution of Sr^{2+} by

Pr^{3+} in small concentrations lowers the polarization due to a decrease of the displacement of the TaO_6 along the polarization direction (*a*-axis). Research to establish the delicate balance between the introduction of vacancies and the optimum Pr doping in SBT leading to increase the remnant polarization is in progress.

Acknowledgments

The authors would like to thank P Casillas, J Palomares, J Peralta, E Aparicio, J A Diaz, J Valenzuela and L Huerta for their technical assistance. J Mata, A Durán and E Martínez also thank the Retention CONACyT programme. This work is partially supported by CONACyT-México, projects 40604-F and 47714-F, and DGAPA-UNAM, projects IN116703 and IN100903.

References

[1] Subbarao E C 1962 *J. Phys. Chem. Solids* **23** 665
[2] Subbarao E C 1962 *J. Am. Ceram. Soc.* **45** 166
[3] Scott J F and Paz de Araujo C A 1989 *Science* **246** 1400
[4] Paz de Araujo C A, Cuchiaro J D, McMillan L D, Scott M C and Scott J F 1995 *Nature* **374** 627
[5] Rae A D, Thompson J G and Withers R L 1992 *Acta Crystallogr.* B **48** 418
[6] Perez-Mato J M, Arroyo M, Garcia A, Blaha P, Schwarz K, Schweifer J and Parlinki K 2004 *Phys. Rev.* B **70** 214111
[7] Blake S M, Falconer M J, McCreedy M and Lightfoot P 1997 *J. Mater. Chem.* **7** 1609
[8] Ismundar and Kennedy B J 1999 *J. Mater. Chem.* **9** 541
[9] Macquart R, Kennedy B J and Shimakawa Y 2001 *J. Solid State. Chem.* **160** 174
[10] Forbess M S, Seraji S, Wu Y, Nguyen C P and Cao G Z 2000 *Appl. Phys. Lett.* **76** 2934
[11] Millan P, Ramírez A and Castro A 1995 *J. Mater. Sci. Lett.* **14** 1657
[12] Noguchi Y, Miyayama M, Oikawa K, Kamiyama T, Osada M and Kakihana M 2002 *Japan. J. Appl. Phys.* **41** 7062
[13] Noguchi Y, Miyayama M, Oikawa K and Kamiyama T 2004 *J. Appl. Phys.* **95** 4261
[14] Noguchi Y, Kitamura A, Woo L-C, Miyayama M, Oikawa K and Kamiyama T 2003 *J. Appl. Phys.* **94** 6749
[15] Wills A S and Brown I D 1999 *QUANTO (A Rietveld Program for Quantitative Phase Analysis of Polycrystalline Mixtures) VaList, CEA, France*
[16] Noguchi Y, Miyayama M and Kudo T 2001 *Phys. Rev.* B **63** 214102
[17] Shimakawa Y, Kubo Y, Nakagawa Y, Kamiyama T, Asano H and Izumi F 1999 *Appl. Phys. Lett.* **74** 1904
[18] Shannon R D 1976 *Acta Crystallogr.* A **32** 751
[19] Hervoches C H, Irvine J T S and Lightfoot P 2001 *Phys. Rev.* B **64** 100102
[20] Durán A, Martínez E, Díaz J A and Siqueiros J 2005 *J. Appl. Phys.* **97** 104109
[21] Brown I D and Altermatt D 1985 *Acta Crystallogr.* B **41** 244
Brown I D 1981 *Structure and Bonding in Crystals* vol 1, ed M O'Keefe and A Navrotsky (New York: Academic)
[22] Brese N E and O'keefe M 1991 *Acta Crystallogr.* B **47** 192
Brown I D 1992 *Acta Crystallogr.* B **48** 553
[23] Shimakawa Y, Kubo Y, Nakagawa Y, Goto S, Kamiyama T, Asano H and Izumi F 2000 *Phys. Rev.* B **61** 6559
[24] Boullay Ph, Trolliard G, Mercurio D, Perez-Mato J M and Elcoro L 2002 *J. Solid State Chem.* **164** 252
[25] Xu Y 1991 *Ferroelectrics Materials and Their Applications* vol 15 (Amsterdam: North-Holland)
[26] Noguchi T, Hase T and Miyasaka Y 1996 *Japan. J. Appl. Phys.* **35** 4900